Journal of Ceramic Processing Research. Vol. 27, No. 1, pp. 48~60 (2026)
(Received 12 August 2025, Received in revised form 25 November 2025, Accepted 22 December 2025)
https://doi.org/10.36410/jcpr.2026.27.1.48

J O U R N A L O F
Ceramic Processing Research

Influence of substitution of red mud on the properties of LC^3 cement

Lingyu Zhang, Yuwu Sui*, Xianglong Meng, Yiwei Fu, Zhibo Zhang, Jialiang Wei, Zhixian Wang, Xiangman Deng and Shaoqi Zhang
School of Materials Science and Engineering of Shandong Jianzhu University, Jinan 250101, China

In 2024, the Royal Swedish Institute of Technology introduced Limestone Calcined Clay Cement (LC^3), which garnered global attention due to its significantly reduced carbon emissions. LC^3 is formulated from clinker, calcined clay (metakaolin, MK), and calcium carbonate (CC). However, with the dwindling reserves of clay and limestone in countries like China and the increasing accumulation of industrial waste such as red mud (RM), substituting RM for MK and CC in LC^3 presents a promising alternative. This study investigated the influence of replacing MK and CC with RM on the properties of mortar, alkali penetration, and microstructure. X-ray diffraction (XRD) was employed to analyze mineral composition, scanning electron microscopy (SEM) to examine microstructure, and energy-dispersive X-ray spectroscopy (EDS) to assess elemental distribution and alkalinity. The results indicate that RM enhances fluidity, prolongs setting time, and increases compressive strength, albeit at the expense of early flexural strength. SEM observations reveal denser composites attributed to the formation of C-A-H and C-A-S-H gels, while EDS analysis shows that ammonium carbonate mitigates calcium ion migration.

Keywords: Limestone calcined clay cement, Red mud, Alkalinity, Metakaolin, Hydrated aluminum calcium silicate.

Introduction

Portland cement, as one of the most widely used building materials in global construction and infrastructure projects, is consumed in enormous quantities. According to data from the United States Geological Survey (USGS), the global cement consumption is currently estimated at 3-4 billion tons per year [1], generating annual CO_2 emissions of approximately 2.5-3.6 billion tons [2].

Portland cement (PC) comprises 95% clinker [3]. The primary source of carbon emissions stems from limestone decomposition, releasing CO_2 during clinker production via calcination [4]. LC^3 cement replaces nearly 50% of clinker with calcined clay (primarily metakaolin [5]) and limestone (calcium carbonate) [6]. Developed by the Swiss Federal Institute of Technology through detailed research (first published in 2024 [5]), this low-carbon cement achieves an effective reduction in CO_2 emissions. Compared to limestone, kaolin contains less carbonate and generates less CO_2 during calcination.

Compared to the early-stage research in China [7-18], which initially focused on preparation technology and performance evaluation, LC^3 cement has been widely implemented in Cuba, India, Nigeria, Pakistan, and Nepal [5, 19]. International researchers have focused on conducting in-depth studies on LC^3 cement. Dhandapani et al. [20] investigated the evolution of pore structures in LC^3 cementitious systems and their impact on performance. Their study demonstrated that LC^3 cement exhibits a highly refined pore structure at early stages, with a strong correlation between electrical conductivity, threshold values, and critical pore sizes. After 7 days of curing, the average pore size decreased significantly. Mishra et al. [21] studied the effect of temperature on LC^3 cement mortar microstructure, observing that at 50 °C (accelerated curing conditions), unevenly distributed hydration products led to larger pores. Compared with ordinary Portland cement, the increased temperature had a more pronounced effect on LC^3 cement porosity.

Kaolin and limestone utilized for replacing clinker in LC^3 cement are important natural mineral resources and are mined excessively [22-24], they are replaced by similar materials in LC^3 are urgently studied. Sunghun Her et al. [25] investigated the feasibility of using oyster shells instead of limestone in the LC^3 system by gauging the hydration reaction and strength of oyster shell calcined clay cement (OC^3). The results certified that OC^3 had a faster hydration and a significant increase of early strength because of a larger specific surface area of oyster shell. Hussam Alghamdi et al. [26] prepared a mixed lightweight LC^3 mortar by replacing natural sand with recycled fine aggregate derived from autoclaved aerated concrete waste (AACW) in different proportions, compared with those of ordinary LC^3 mortar, the workability, and the thermal conductivity, early compressive strength, and tensile strength of LC^3-AACW composite were significantly reduced with the

*Corresponding author:
Tel : +86 13864183731
Fax: +86 0531 86367282
E-mail: herrsui@sdjzu.edu.cn

increase of AACW aggregate, but they still met the EN 998-1 standard. Yuchen Hu et al. [27] employed calcined marine clay to replace the metakaolin in LC^3-50 and LC^3-70 systems at different ratios, the results indicated that the early compressive strength of all mixed mortars substituted by calcined marine clay lower, displayed more intricate microstructures and greater porosity, notably, the incorporation of calcined marine clay in the LC^3-50 system enhanced its resistance to chloride infiltration. Junjie Hu et al. [28] used incineration fly ash (IFA) and CO_2-active IFA (CIFA) in different proportions to substitute limestone in LC^3 cement, experimental results indicated that the incorporation of IFA hindered the system's early hydration. In comparison to LC^3 cement, there was a reduction in early compressive strength, however, an elevation in later compressive strength. The LC^3-CIFA composite demonstrated an enhanced hydration activity, with its compressive strength in both early and later stages significantly surpassing that of LC^3 cement and the LC^3-IFA composite.

Red mud, the solid waste with huge emissions in the world [29], is an accessory in the production process of refined alumina from bauxite [29], round 1.0-1.8 tons of red mud is made from every ton of alumina production. Red mud exhibits strong alkalinity due to sodium oxide and other components inside, causing great damage to soil [30]. However, the utilization of red mud is relatively difficult, the harmless utilization of red mud is a problem in the whole world. Among the various recycling methods of red mud, the utilization as building materials is considered the most effective way due to its high demand and low processing cost [31].

Previously, many researchers have experimentally studied the properties of the ordinary concrete with the addition of RM [32-37], some positive influences are gotten, nevertheless, presenting alkalinity is difficultly solved. However, to date, no studies have systematically investigated the optimal ratio for preparing LC^3 cement using red mud. Additionally, the high alkalinity of red mud remains a critical issue that requires urgent attention. There is a pressing need for simpler and more efficient pretreatment methods to enhance the reactivity of red mud. In this study, red mud refined by ball milling and screening was used to replace metakaolin (10%, 20%, 30%) and calcium carbonate (5%, 10%, 15%) in LC_3 cement, respectively, to investigate the properties of the composite. The inhibitory effect on alkalinities was further validated by incorporating 15% ammonium carbonate as an additional measure. The study experimentally examined the fundamental properties, including of fluidity, initial and final setting, mechanical properties, as well as the presenting alkalinity resistance of the composite. Additionally, XRD, EDS and SEM are employed to analyze the hydration mechanism and microstructure of the composite. The aim of this study is to investigate the use of RM in LC^3, reduce use of natural resources.

Materials, Program and Methods

Materials

The RM used in this study was recovered from a factory producing alumina in Binzhou city of China, it was initially ground in a ball mill, then sieved through a 100-mesh sieve to obtain the experimental materials. The RM is crimson in color and has strong alkalinity [29], it is mainly composed of Fe_2O_3, $Al2O_3$, SiO_2, Na_2O and other oxides, naturally Na_2O exists in RM by the form of NaOH resulting in high alkalinity of RM (Seen in Table 1). MK and CC are both bought and are white powders, among which MK is mainly composed of SiO_2, Al_2O_3 and so on (Seen in Table 1). CaO and CO_2 are the main compositions of limestone (Seen in Table 1). XRF devices are utilized to detect elements, which are typically represented in the form of oxides. The carbon element is expressed as CO_2 and primarily originates from the decomposition of $CaCO_3$.The clinker obtained from the cement factory in Jinan City is gray, mainly composed of CaO, SiO_2 and Al_2O_3 (Seen in Table 1).

Distributions of particle size of RM, MK and CC used in the experiment are detected and shown in Fig. 1, the average particle size and volume specific surface area are demonstrated in Fig. 2. The average particle size of red mud particles is larger than that of metakaolin and smaller than that of calcium carbonate. The maximum specific surface area indicates that the shape of red mud particles is irregular. Combined with SEM images (seen Fig. 3), it can be seen that the surface of red mud particles is rough.

The mineral compositions of MK, CC and RM are tested by XRD and the results reveal that they mainly contain mullite, $CaCO_3$ and hematite, respectively, moreover, some Amorphous materials exist in RM and MK (seen Fig. 4).

In addition to basic materials such as RM, cement clinker, MK, CC, and gypsum, the ammonium carbonate

Table 1. Chemical composition and content of red mud, metakaolin, calcium carbonate and clinker (%).

	CaO	SiO_2	CO_2	Al_2O_3	Fe_2O_3	Na_2O	Others
Clinker	48.273	20.827	11.635	9.052	3.931	-	6.282
CC	55.153	1.986	40.988	0.748	0.358	-	0.767
MK	0.209	49.646	3.778	44.287	0.504	-	1.576
RM	2.614	12.565	8.979	21.904	38.801	7.418	7.719

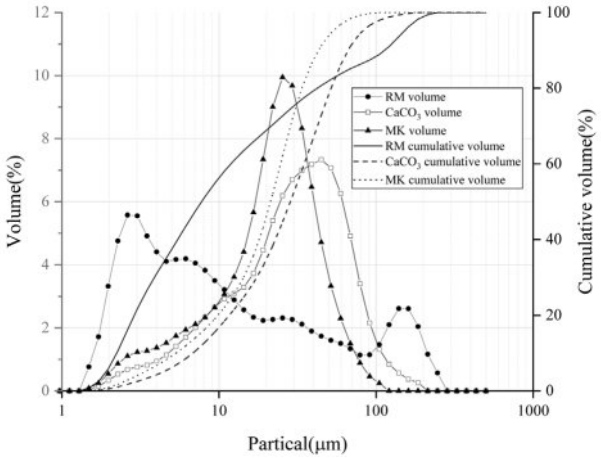

Fig. 1. Particles distribution of RM, MK and CC.

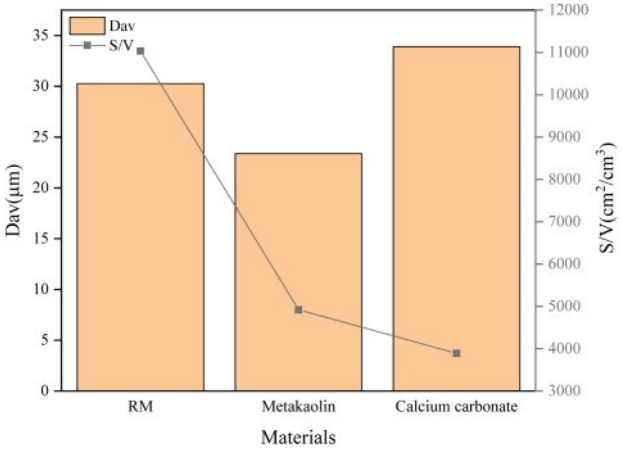

Fig. 2. Average particle size, specific volume surface area of RM, MK and CC.

(AC) is utilized to reduce the alkalinity of red mud.

Mix proportion

The control sample in this study is the LC^3-50 system, which consists of 50% clinker, 30% metakaolin, 15% calcium carbonate, and 5% gypsum.

In this study, 10%, 20%, 30% MK and 5%, 10%, 15% CC are replaced by RM respectively. And in order to study the alkalinity of red mud, 15% ammonium carbonate is added to each group containing red mud as a control agent to inhibit alkalinity. The specific recipe is shown in Table 2.

Experimental methods

The fluidity of mortar was measured using a cement mortar fluidity tester in accordance with the national standard GB/T 2419 [38]. After wiping the jumping table

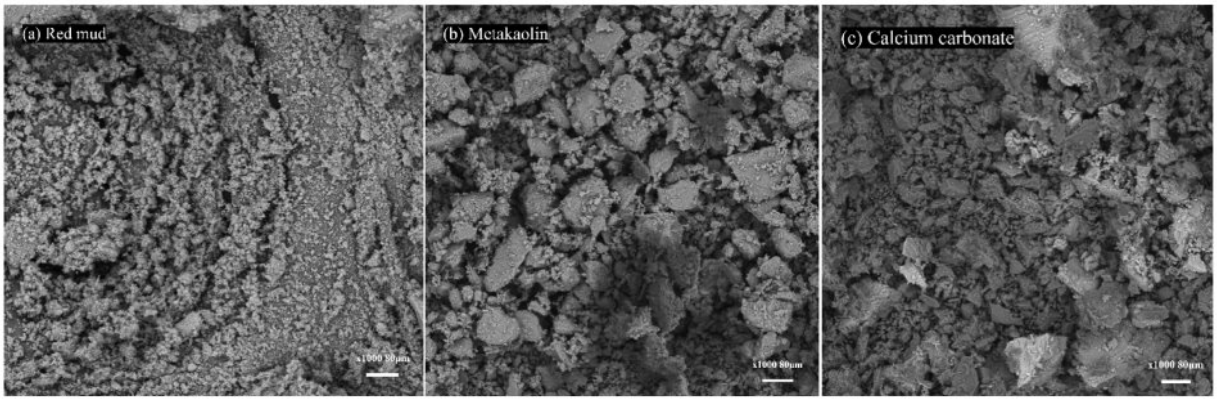

Fig. 3. Structure and morphology of RM, MK and CC detected by SEM detection.

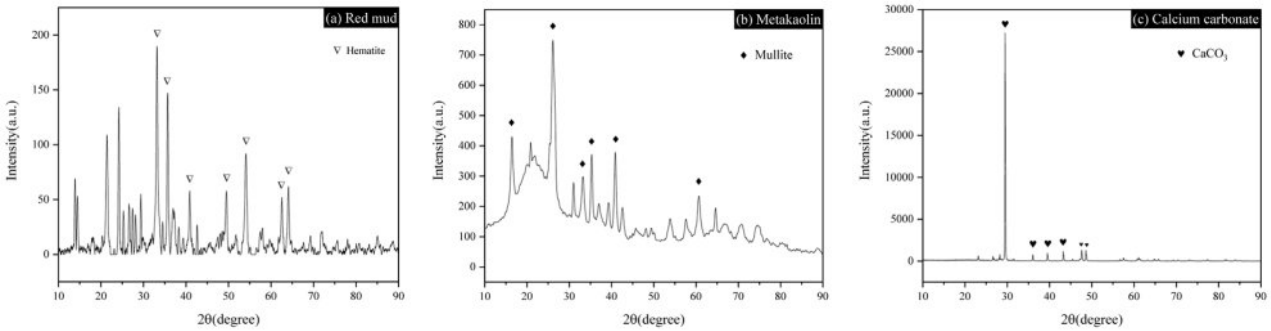

Fig. 4. Mineral composition of RM, MK and CC detected by XRD.

Table 2. Experimental mortar recipe.

Sample ID	Clinker (%)	MK (%)	$CaCO_3$ (%)	RM (%)	Gypsum (%)	$(NH_4)_2CO_3$ (LC^3%)	Water/LC^3 ratio	LC^3/IOS sand ratio
1	50	30	15	0	5	0		
2	50	20	15	10	5	0		
3	50	10	15	20	5	0		
4	50	0	15	30	5	0		
5	50	30	10	5	5	0		
6	50	30	5	10	5	0		
7	50	30	0	15	5	0	0.55	1:3
8	50	20	15	10	5	15		
9	50	10	15	20	5	15		
10	50	0	15	30	5	15		
11	50	30	10	5	5	15		
12	50	30	5	10	5	15		
13	50	30	0	15	5	15		

surface, inner wall of the trial mold, and ramming rod with a damp towel, the mixed mortar was quickly poured into the trial mold in two layers. After compacting, the mold was removed and the jumping table was vibrated 25 times within 25 s±1 s. The diameter of the mortar was measured in perpendicular directions with a trisquare, and the average of three measurements was recorded for each group.

Once the mortar was thoroughly mixed using a cement mortar mixer, it was carefully placed in a 40 mm×40 mm×160 mm cement mortar mold. Subsequently, in accordance with JJF 1867 [39], it was precisely shaped on a cement mortar compaction test stand and wrapped in plastic film for curing at room temperature. Demolding occurred one day later. Post-demolding, the test blocks were transferred to a standard curing chamber maintained at 20 °C±1 °C with controlled humidity.

The mechanical strength of the composite mortar was determined according to GB/T 17671 [40]. The bending strength and compressive strength of the test blocks at 3d, 7d, and 28d were measured using a DKZ-5000 cement electric bending tester (Cangzhou, China) and a YAW-300B automatic press (Jinan, China). The bending strength was tested on one cuboid block, followed by compressive strength tests on two broken blocks. The final results were averaged for graphical analysis.

The setting time and soundness of cement were tested using standard consistency paste according to GB/T 1346 [41]. For setting time measurement, the paste was filled into a test mold on a glass plate and smoothed. The mold was maintained in a constant temperature/humidity chamber. The initial and final setting times were determined with a Vicat apparatus using respective test needles. For soundness testing, the standard paste was applied with a spatula onto an oil-coated glass plate to form a test cake, which was cured for 24±2 h. After removing the glass plate, the cake was heated in a boiling box for 30±5 min until boiling, then held for 180±5 min. Cracking and warping of the test cake were observed and documented.

To investigate red mud's effects on alkali efflorescence and ammonium carbonate's inhibitory role, 28-day-cured mortar specimens were broken into small pieces of uniform size/weight. These pieces were immersed in equal volumes of deionized water for 24 hours. The pH values of the leachate were monitored daily using a portable pH meter.

In this study, a Phenom Pharos G2 benchtop FE-SEM (Thermo Fisher Scientific, Netherlands) and an X'PERT³ MRD XRD system (Malvern Panalytical, UK) were employed to analyze the mineral composition and microstructure of composite mortar. An EDS detector coupled with SEM was used to map elemental distributions, enabling exploration of red mud's impact on caustic penetration in the mortar.

Results and Discussion

Fluidity, setting time and stability of mortars

Figure 5 shows the fluidity and setting time of mortars when RM replaces MK and CC, respectively. As can be seen from Fig. 5(a), the substitution of RM improves the fluidity of composite by 3.23%, 1.61% and 0.54%, when the replacement amount is 10%, 20% and 30% due to its fineness and low viscosity, but the fluidity gradually decreases with the increase of RM content when MK is replaced. When RM replaces CC by 5%, 10% and 15%, the fluidity increases by 22%, 8.6% and 6.45%, respectively. The maximum fluidity reaches 227 mm.

The differences in fluidity observed when red mud replaces calcium carbonate and calcined kaolin are related to its particle morphology, along with the interactions

between Na_2O, Fe_2O_3 and water. Initially, the addition of a small amount of very fine RM particles to partially replace MK allows them to fill the voids between MK particles. This micro-aggregate effect enhances the particle packing density, leading to more free water available in the paste under a constant water-to-binder ratio and consequently an improvement in fluidity. With a further increase in the RM substitution level, the effects of the soluble alkali (Na_2O) and iron phase (Fe_2O_3) abundant in RM become more pronounced. Na_2O dissolves rapidly, increasing the alkalinity of the liquid phase in the paste, which may promote early-age hydration reactions and consume free water; Fe_2O_3, which typically exists in forms such as hematite, possesses complex surface chemistry and exhibits a strong adsorption effect on water molecules. Simply put, the substitution of MK with RM exhibits an optimal dosage. Within this range, RM acts beneficially as a filler, but beyond it, its detrimental effect as a highly water-absorbing active powder dominates. In the paste, CC is typically regarded as an inert filler. It is characterized by its regular particle morphology, inert surface chemistry, and consequently, a very low water demand. The replacement of CC with RM replaces an ideal filler with a material exhibiting high water requirements, irregular morphology, and surface reactivity. This, together with the roles of Na_2O and Fe_2O_3, consequently causes a drastic reduction in fluidity. The inherently low packing density (due to coarse CC particles and a missing mid-size fraction) and high water demand of the CC system is greatly improved initially by RM's particle packing effect, causing the initial fluidity surge. This benefit, however, is gradually offset as the negative chemical effects of RM increase linearly with its dosage.

Figure 5(b) demonstrates that when RM replaces MK, the initial and final setting time of the composite also increase with the replacement amount enhance. When the replacement amount is 30%, the initial setting time is increased by 56.7%, and the final setting time is increased by 19.3%. The results from Fig. 5(c) show that when CC

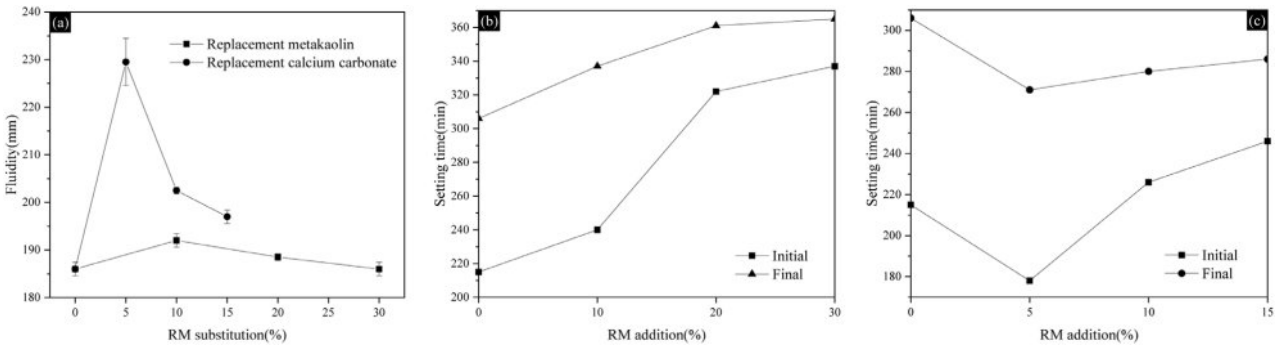

Fig. 5. Influence of RM on the fluidity and the setting time of composites. (a) RM replacement influence on fluidities; (b) Setting time of replacing MK with RM; (c) Setting time of replacing CC with RM.

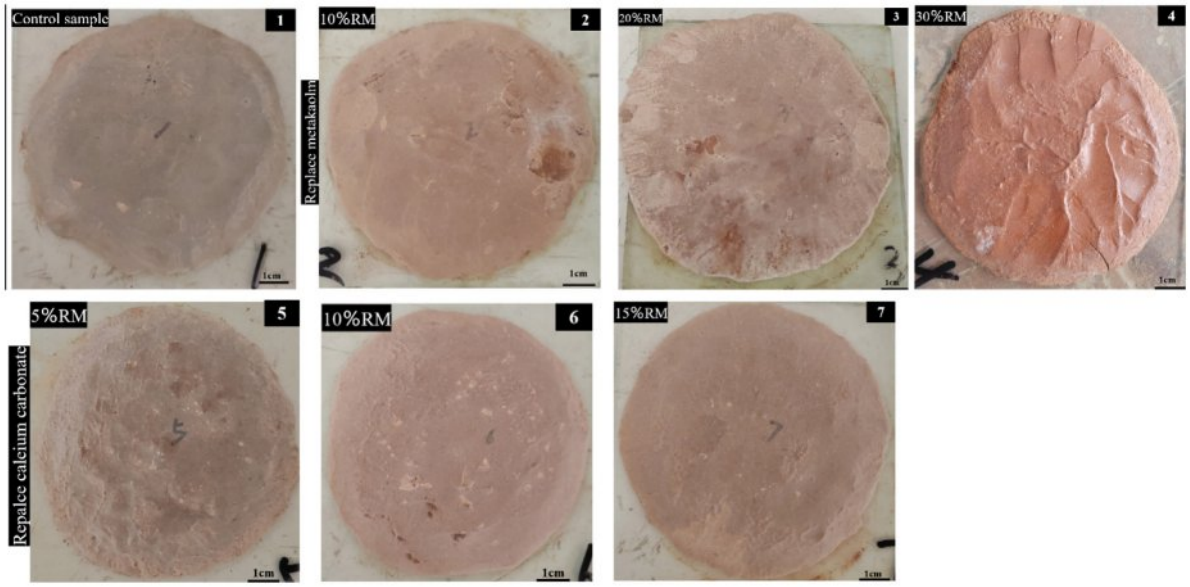

Fig. 6. Stability test results of composite (The image labels are the same as the sample IDs in Table 2).

is replaced by RM, the initial and final setting time of the composite decreases firstly and then increases with more replacement amounts. When CC is replaced by RM totally, the initial setting time is increased by 14.4% and the final setting time is reduced by 6.5%. Because the size distribution of red mud is not uniform and some are relatively large, the reaction efficiency is reduced and the hydration process is delayed. Additionally, the rough surface of red mud hinders the agglomeration of cement particles and hydration products, thereby affecting the setting time.

The stability test results of the cement paste are shown in Fig. 6. From the macroscopic observations of the test cakes, it is evident that none of the samples exhibited severe cracking or warping after being boiled. This suggests that the incorporation of red mud does not compromise dimensional stability. As the dosage of red mud increases, the surface roughness also increases, resulting from the unreacted red mud particles forming micro-protrusions on the surface.

Strengths of composites

Figure 7 shows the changes of flexural strength and compressive strength at 3-d,7-d and 28-d with RM replacement of MK and CC. For the flexural strength, the RM replacement improves the early strength of composite, but negatively affects 28-d strength for the composite which MK is replaced by RM. With the

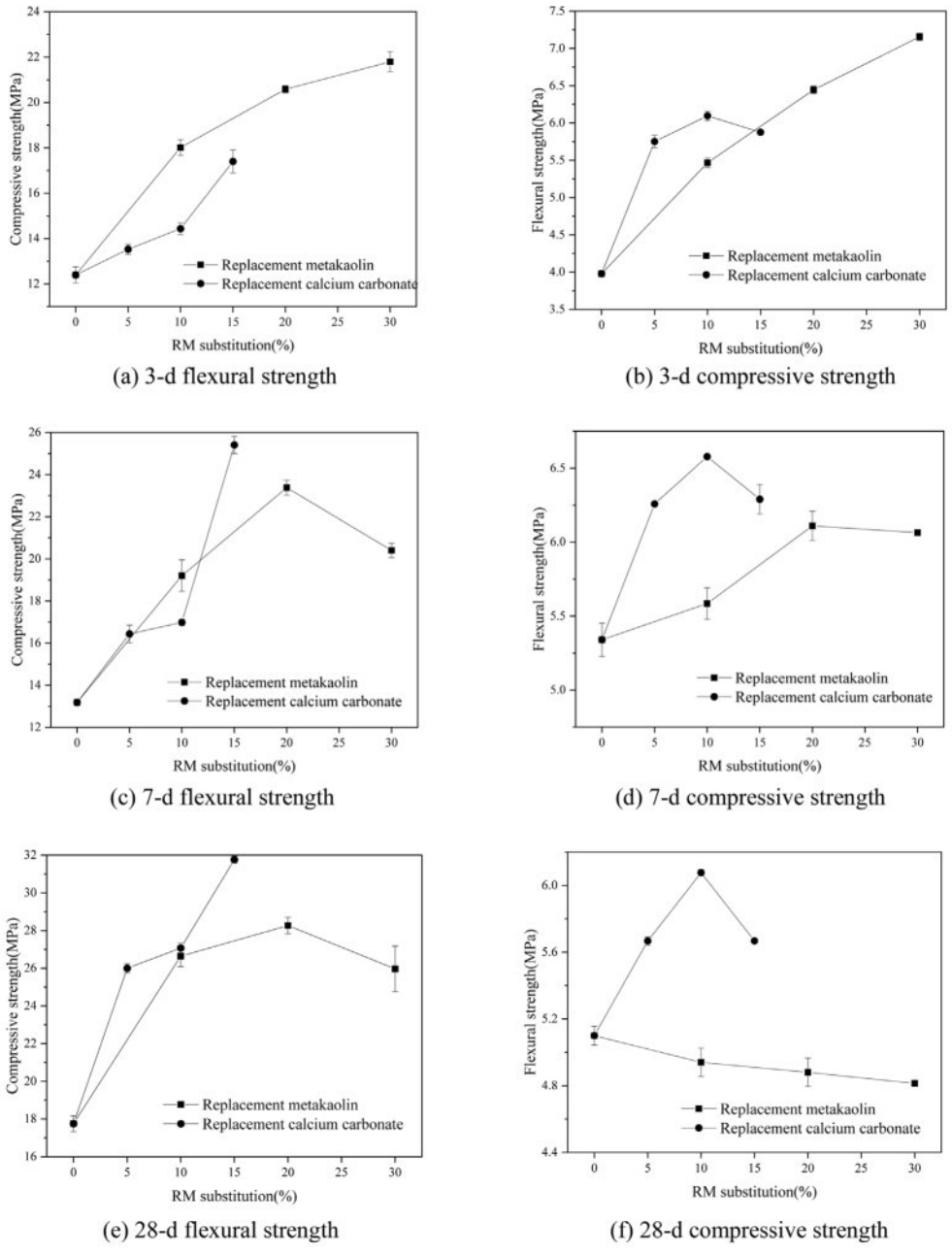

Fig. 7. Influence of RM on the 3-d,7-d, 28-d strengths of composites.

increase of RM replacement of MK, the 3-d flexural strength is significantly increased, the maximum of increase is 79.6% (Seen Fig. 7(a)). The 7-d strength increases firstly and then decreases; the maximum of increase is 15.3% by the 20% replacement amount (Fig. 7(c)). The 28-d strength is slightly decreased with 5.7% (Fig. 7(e)). With the substitute increase of RM for CC, the 3-d,7-d, and 28-d flexural strengths fairly increase with more RM replacement, as the replacement amount 10%, the increase percentage is 53.3%, 24.2% and 19.2%, respectively (Fig. 7(a, c, e)). When the RM substitutes MK, the 3-d compressive strength increases highly with the enhance of replacement amount, and the maximum increase percentage is 75.8% (Fig. 7(b)). The 7-d and 28-d compressive strengths increase firstly and then decrease, as 20% replacement amount, the increase percentages are 77.3% and 59.2%, respectively (Fig. 7(d, f)). When RM replaces CC, the compressive strength of 3,7,28 days increase significantly with the replacement increase, however, the values of 10% substitute amount are similar compared with the 5% replacement. When RM completely replaces CC, the compressive strengths of 3,7,28 days increase by 40.4%, 92.7 % and 78.9%, respectively (Fig. 7(b, d, f)).

Influence of red mud on the alkalinities

Alkali metal ions, such as sodium ions, present in red mud adsorb onto the surface of cement particles, forming a charged adsorption layer. This layer inhibits the contact reaction between cement particles and water, thereby explaining the prolonged setting time. Furthermore, the dissolution, migration, and potential precipitation crystallization of these alkali metal ions can lead to the formation of non-uniform pore and channel distributions within the cement matrix. Some hydroxide ions in the composite mortar are dissolved in water and react with calcium and sodium ions to form calcium hydroxide and sodium hydroxide. As water evaporates, these compounds migrate through the internal pores of the mortar and precipitate as a white powder on its surface. The presence of a slight white powder on the surface of the red mud-modified mortar test blocks is shown in Fig. 11.

After 28 days the mortars are broken into small pieces of the same size (without grinding) and soaked in the same amount of deionized water. Fig. 8 shows the change of pH value of the leaching solution, when the RM replaces MK and CC with or without ammonium carbonate. Obviously demonstrate that compared with the control sample, the substitute of RM can enhance the pH value because RM contains alkaline material, the addition of AC can react with sodium hydroxide in RM (Seen formula (1)) and reduce the alkaline content.

$$(NH_4)_2CO_3 + NaOH \rightarrow Na_2CO_3 + NH_3\uparrow + H_2O \quad (1)$$

Figure 8 demonstrates that the addition of AC can significantly reduce the alkalinity introduced by RM, with the extent of reduction being positively correlated with the replacement ratio of RM. Specifically, a higher proportion of RM leads to a more pronounced alkalinity-reducing effect of AC. Throughout the entire 18-day observation period, the pH curve of the sample with AC for any given RM ratio was consistently lower than that of its counterpart without AC. This clearly confirms the continuous and effective neutralizing effect of AC. A pH reduction of 0.2 to 1.0 units was observed upon the addition of ammonium carbonate, with its effectiveness varying according to the RM ratio and the duration. The neutralization effect of ammonium carbonate, however, is not entirely stable. The resulting sodium carbonate (Na_2CO_3) itself is alkaline. Furthermore, it can slowly react with CO_2 and moisture in the system, resulting in a gradual pH rebound following the initial rapid drop. Nonetheless, the addition of AC ultimately

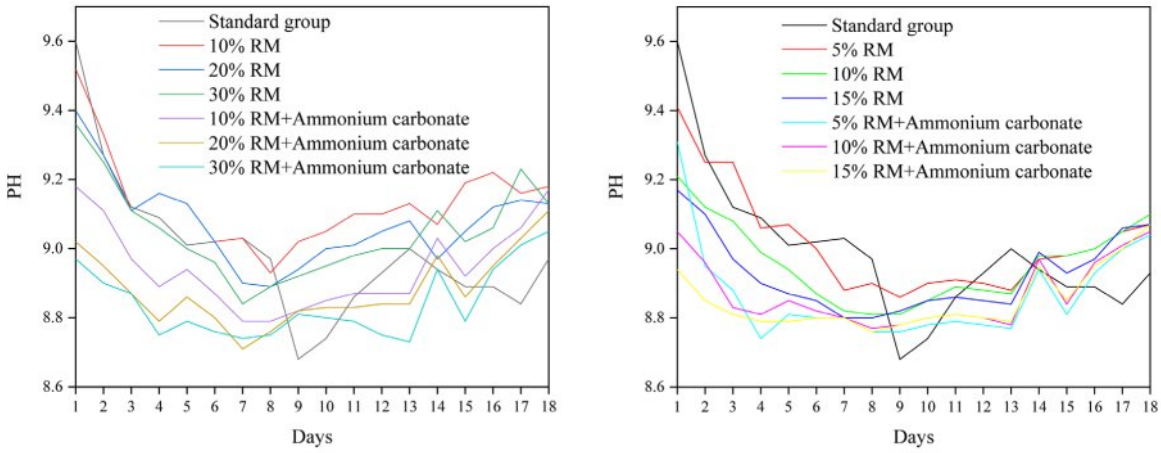

(a) Change of pH value of composite materials with red mud replacing metakaolin

(b) Change of pH value of composite materials with red mud replacing calcium carbonate

Fig. 8. Change of pH value of composite.

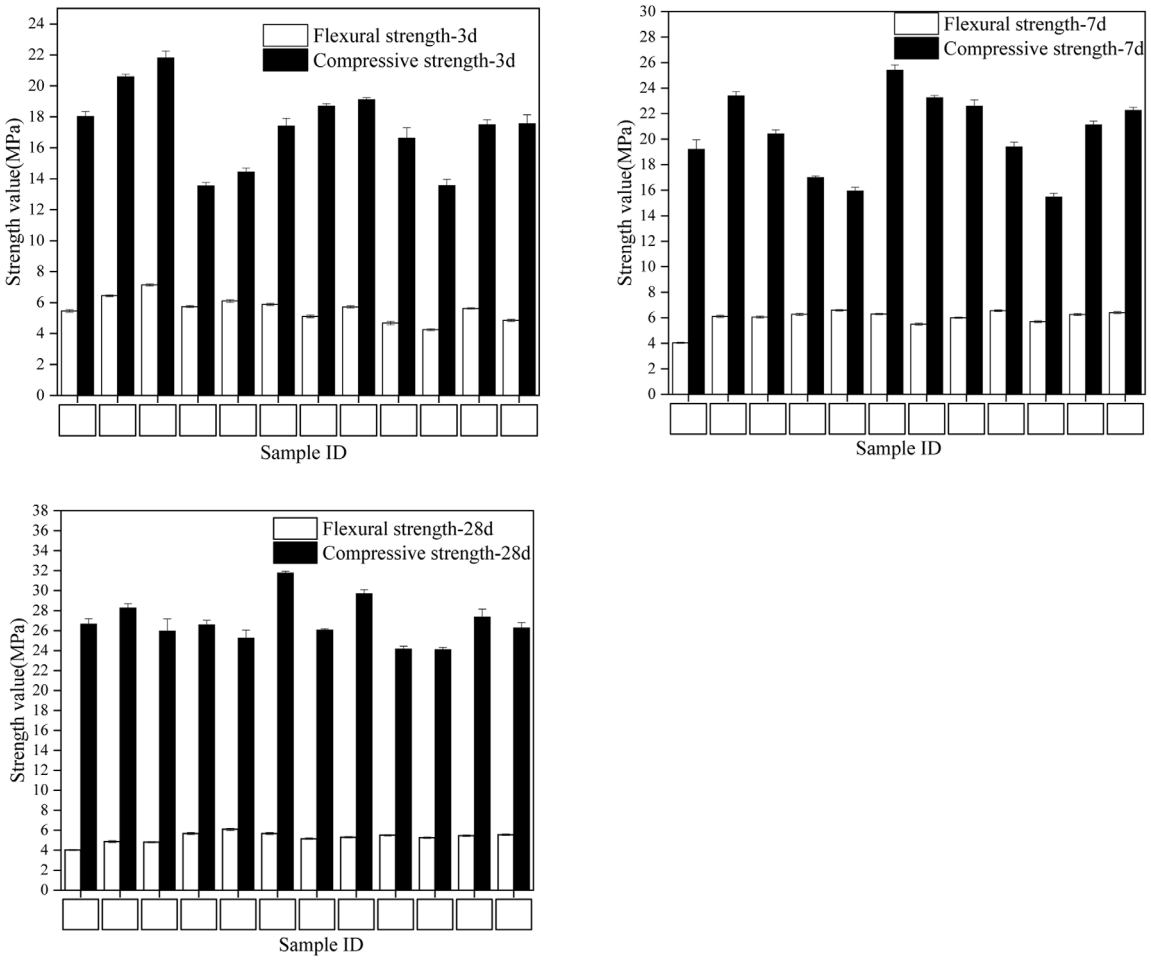

Fig. 9. The 3.7.28-day mechanical performance of composite mortar.

helped maintain a relatively more stable and lower pH throughout the curing period, which is beneficial for controlling the material's long-term alkalinity.

In order to further explore the alkalinity of composite, EDS detection of element distribution and content are performed on the surface and interior of samples with or without RM and AC. Fig. 10 shows the EDS detection results. In Fig. 10(2) the blue color represents calcium ions, rose red represents sodium ions (Seen Fig. 10(3)), and the brighter the color, the more the ion content. Fig. 9(4) demonstrates the elements gauged by EDS, except the element gold (detection usage), the contents of calcium and sodium elements are sorted out in Table 3 (The detection points are marked by Fig. 10(1)). The calcium content in surface of control sample is lower than that of interior, contrarily, calcium element contents in other samples are more in surface than those in interior because of calcium migration to the surface in the curing period. The sodium element content has no obvious change. Compared with the samples without adding AC, the surface sodium content decrease and the internal content increase. However, because $NaCO_3$ has a certain solubility in water, its inhibitory effect on sodium ion migration is not as obvious as that on calcium ions. Additionally, Fig. 1 shows that the white powder on the mortar specimen surface was markedly reduced with the addition of AC. Combined with the subsequent strength tests, it indicates that the long-term strength (following AC inhibition) can approach or be slightly below the initial level under an appropriate RM dosage.

The flexural and compressive strength tests of the composite mortar with AC added are conducted for 3, 7, and 28 days, and the results are shown in Fig. 9. Compared with the composite mortar without ammonium carbonate, the 3-d strength decreased, due to the increase in porosity caused by the generation of NH_3 gas. With the progress of hydration and the formation of $CaCO_3$ precipitation to fill the pores, the 7-d strength recovered, approaching or slightly lower than the original level. For the 28-d strength, stable ion distribution and uniform internal reaction have improved the strength of the group with low red mud content, but the group with high red mud content still has lower strength due to insufficient activity.

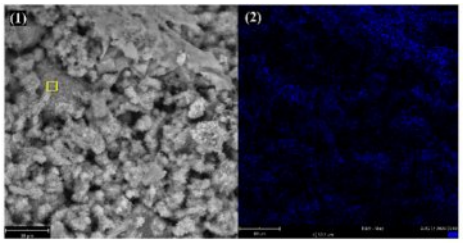

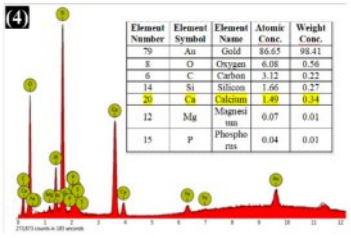

Element Number	Element Symbol	Element Name	Atomic Conc.	Weight Conc.
79	Au	Gold	86.65	98.41
8	O	Oxygen	6.08	0.56
6	C	Carbon	3.12	0.22
14	Si	Silicon	1.66	0.27
20	Ca	Calcium	1.49	0.34
12	Mg	Magnesium	0.07	0.01
15	P	Phosphorus	0.04	0.01

(a) Control sample without RM (Surface)

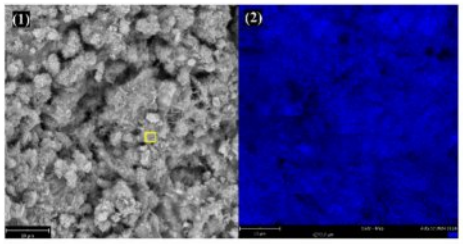

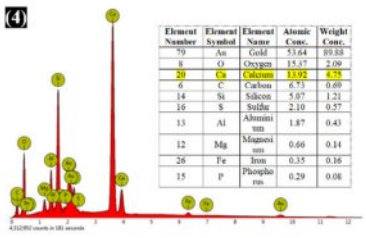

Element Number	Element Symbol	Element Name	Atomic Conc.	Weight Conc.
79	Au	Gold	53.64	89.88
8	O	Oxygen	15.57	2.09
20	Ca	Calcium	13.92	6.75
6	C	Carbon	6.73	0.69
14	Si	Silicon	5.07	1.21
16	S	Sulfur	2.10	0.57
13	Al	Aluminium	1.87	0.43
12	Mg	Magnesium	0.66	0.14
26	Fe	Iron	0.35	0.16
15	P	Phosphorus	0.29	0.08

(b) Control sample without RM (Inside)

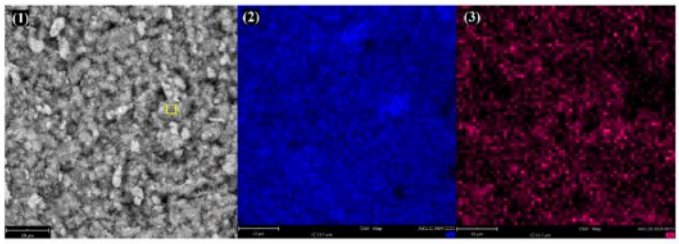

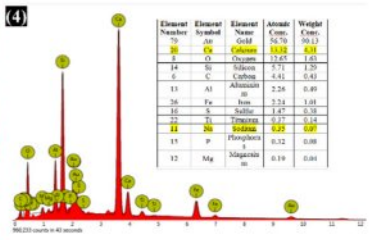

Element Number	Element Symbol	Element Name	Atomic Conc.	Weight Conc.
79	Au	Gold	56.70	90.13
20	Ca	Calcium	13.32	4.31
8	O	Oxygen	12.65	1.63
14	Si	Silicon	5.71	1.29
6	C	Carbon	4.41	0.43
13	Al	Aluminium	2.26	0.49
26	Fe	Iron	2.24	1.01
16	S	Sulfur	1.47	0.38
22	Ti	Titanium	0.37	0.14
11	Na	Sodium	0.23	0.07
15	P	Phosphorus	0.12	0.08
12	Mg	Magnesium	0.19	0.04

(c) Sample substituted MK by 20% RM (Surface)

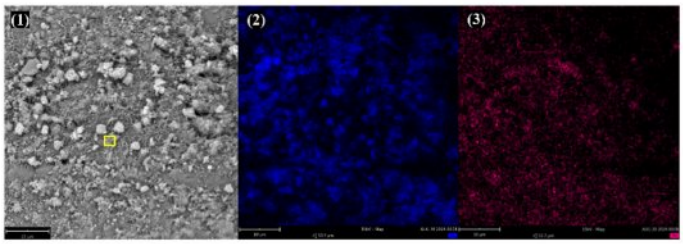

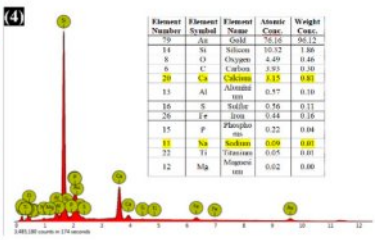

Element Number	Element Symbol	Element Name	Atomic Conc.	Weight Conc.
79	Au	Gold	56.16	90.12
14	Si	Silicon	10.32	1.86
8	O	Oxygen	4.49	0.46
6	C	Carbon	3.95	0.30
20	Ca	Calcium	3.15	0.81
13	Al	Aluminium	0.57	0.10
16	S	Sulfur	0.56	0.11
26	Fe	Iron	0.44	0.16
15	P	Phosphorus	0.22	0.04
11	Na	Sodium	0.09	0.01
22	Ti	Titanium	0.05	0.01
12	Mg	Magnesium	0.02	0.00

(d) Sample substituted MK by 20% RM (Inside)

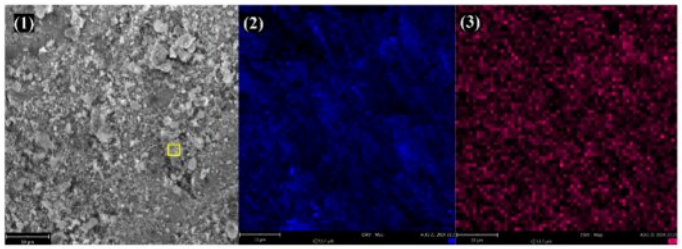

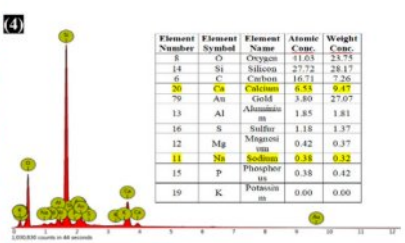

Element Number	Element Symbol	Element Name	Atomic Conc.	Weight Conc.
8	O	Oxygen	41.03	23.75
14	Si	Silicon	27.72	28.17
6	C	Carbon	16.71	7.26
20	Ca	Calcium	6.55	9.47
79	Au	Gold	3.80	27.07
13	Al	Aluminium	1.85	1.81
16	S	Sulfur	1.18	1.37
12	Mg	Magnesium	0.42	0.37
11	Na	Sodium	0.38	0.32
15	P	Phosphorus	0.38	0.42
19	K	Potassium	0.00	0.00

(e) Sample substituted MK by 20% RM and addition 15% AC (Surface)

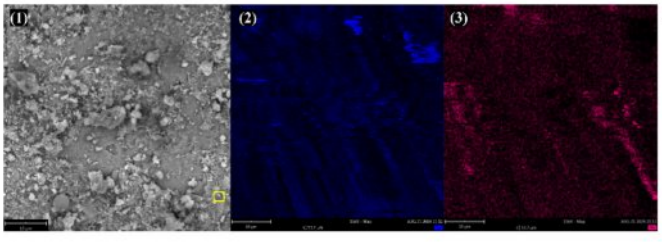

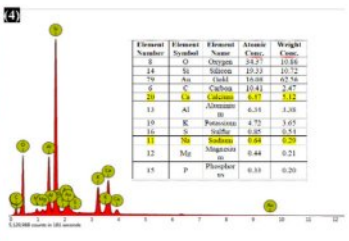

Element Number	Element Symbol	Element Name	Atomic Conc.	Weight Conc.
8	O	Oxygen	34.27	10.86
14	Si	Silicon	19.33	10.72
79	Au	Gold	16.08	65.56
6	C	Carbon	10.41	2.47
20	Ca	Calcium	6.17	5.12
13	Al	Aluminium	6.35	3.38
19	K	Potassium	4.75	3.65
16	S	Sulfur	0.85	0.53
11	Na	Sodium	0.64	0.29
12	Mg	Magnesium	0.44	0.21
15	P	Phosphorus	0.33	0.20

(f) Sample substituted MK by 20% RM and addition 15% AC (Inside)

Fig. 10. EDS test results of composite block surface and inside ((1) SEM image of detection point; (2) Calcium element map; (3) Sodium element map; (4) EDS spectrum and content table of each element).

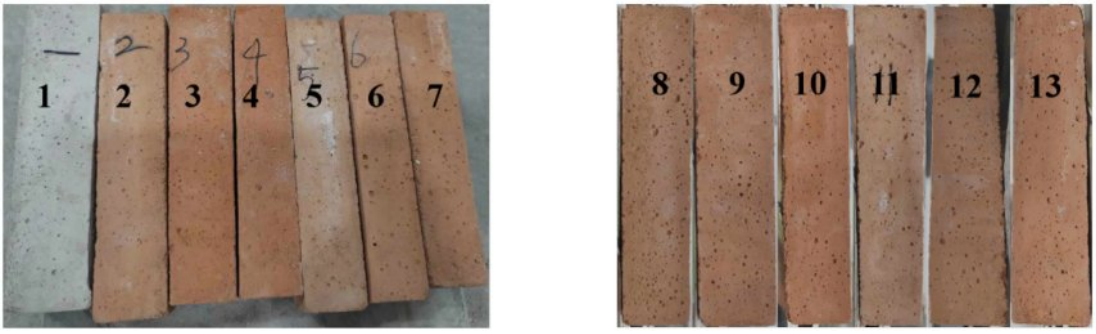

Fig. 11. Composite mortar test blocks (The image labels are the same as the sample IDs in Table 2, The first figure shows the composite mortar test blocks without AC, while the second shows those with AC.)

Table 3. Calcium and sodium atomic content in composites (%).

	Contral sample		Sample replaced by 20%RM		Sample replaced by 20% RM with 15% AC	
Element	Calcium	Sodium	Calcium	Sodium	Calcium	Sodium
Surface	0.1168	0	0.3076	0.0081	0.0679	0.0040
Inside	0.3003	0	0.1321	0.0038	0.0771	0.0076

Mineral composition of composite

The XRD results of the composite cured for 28 days are shown in Fig. 11. The labels in the pictures are the sample IDs in the recipe (Seen in Table 2). In the control sample except C-S-H gel AFt, AFm, C-A-H, C-A-S-H as well as CC appear. More C-A-H phases are generated when RM replaces MK compared with the control sample (Seen Fig. 12(2,3,4)). When RM replaces CC, compared with the control sample, more C-A-S-H phases are formed in mortars (Seen Fig. 12(5,6,7)), moreover, with the increase of red mud, the intensity of Aft phase peak also gradually increases, C-A-S-H appearance certifies the existence of reactive Al_2O_3 and SiO_2, they can react with $Ca(OH)_2$ (Seen formula 2) [42]

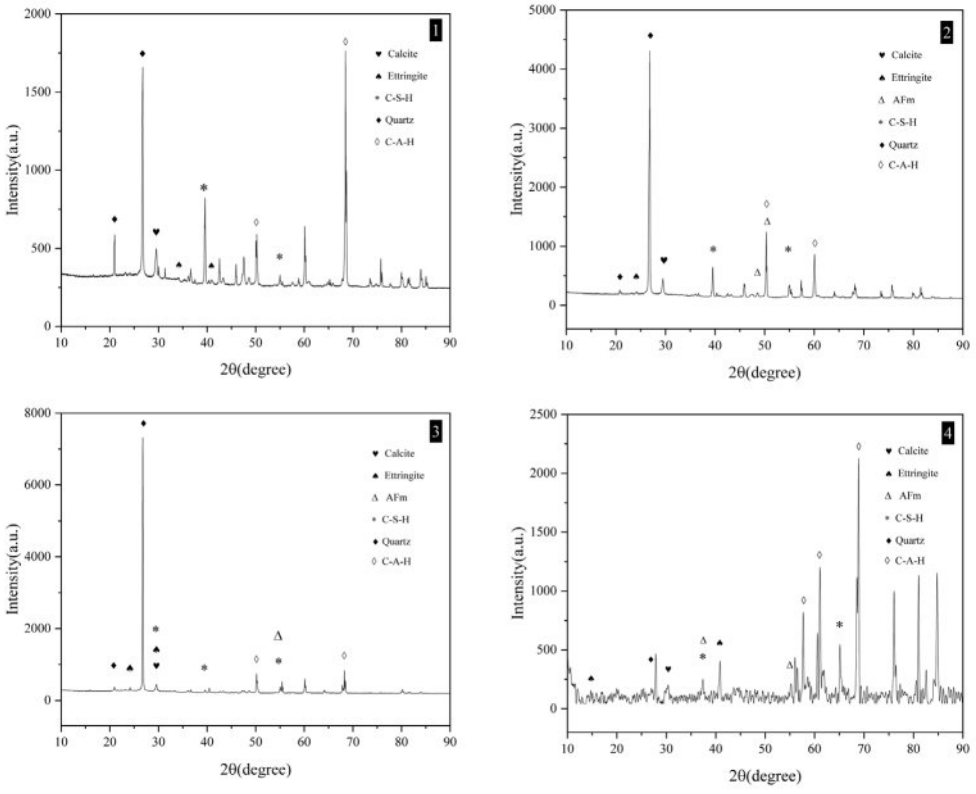

Fig. 12. Mineral composition of mortars detected by XRD (The image labels are the same as the sample IDs in Table 2).

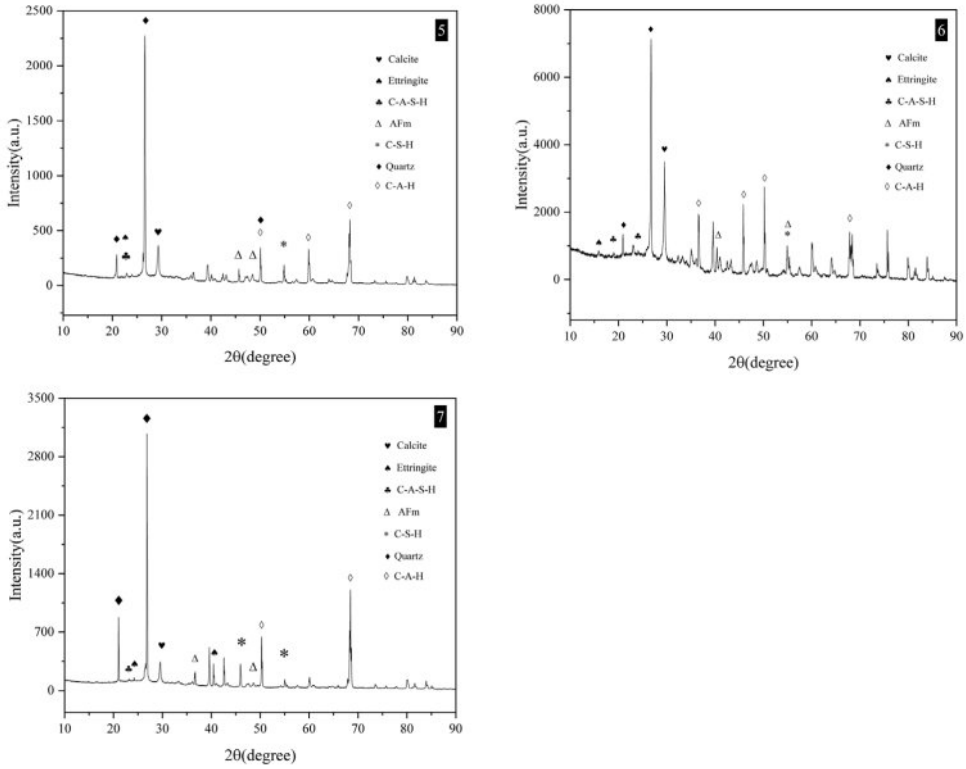

Fig. 12. Continued.

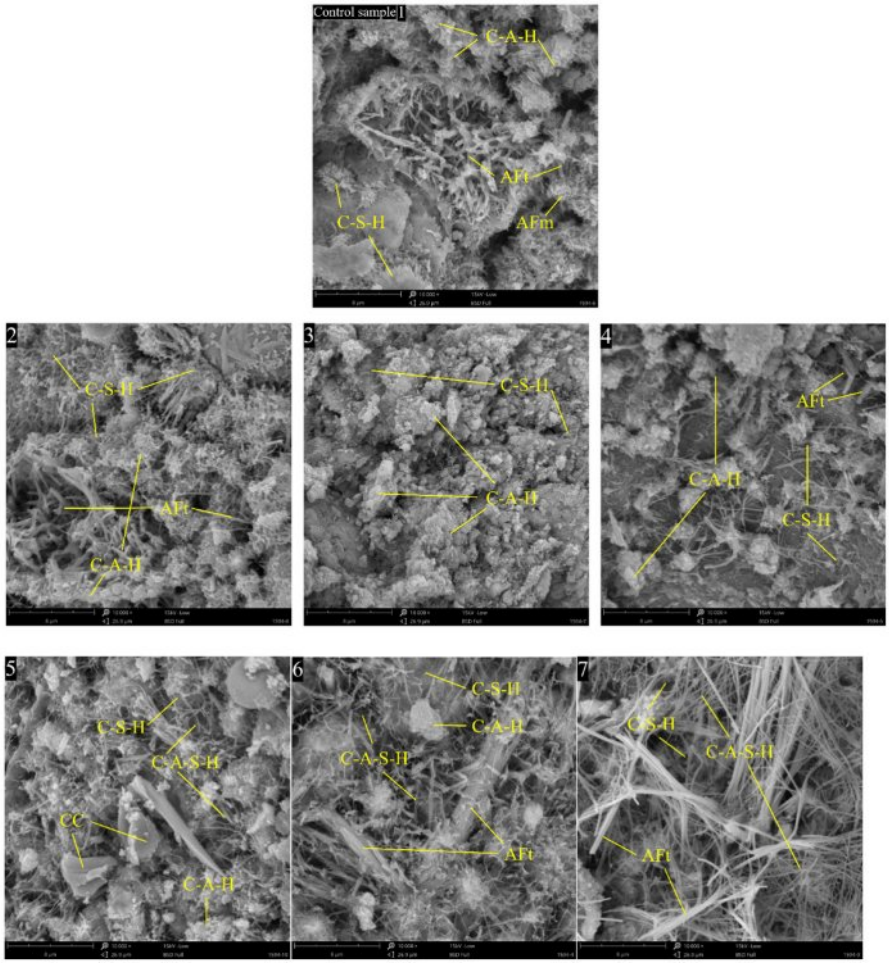

Fig. 13. Structure and morphology of composite detected by SEM (The image labels are the same as the sample IDs in Table 2).

and promote to strengthen the mortars.

$$Al_2O_3+2SiO_2+Ca(OH)_2+8H_2O \rightarrow CaO\cdot Al_2O_3\cdot 2SiO_2\cdot 9H_2O(C\text{-}A\text{-}S\text{-}H) \quad (2)$$

Structure and morphology of mortars

The SEM gauging results of the mortars cured for 28 days are shown in Fig. 13. The labels in the pictures are the sample IDs in the recipe (Seen Table 2). In control sample floc-like C-S-H and rodlike AFt grow thickly, C-A-H gel, flake shaped C-A-S-H gel, AFm and $CaCO_3$ crystals can be seen, pores appear in the structure (Fig. 13(1)). With the substitution of MK by RM from 10% to 30% (Fig. 13(2-4)) AFt reduces, C-A-H gel increases, and a few cracks and pores represent, the structures are compacted. The hydrated calcium silicate crystals interweave with one another to form a complex spatial network, thereby enhancing the compactness of the cement matrix and making a significant contribution to the development of early strength. However, excessive C-A-H can cause agglomeration, leading to a rebound in porosity, weakening the interface area, and becoming the crack initiation point under tensile stress. This also explains why the flexural strength at 28 days has decreased. When RM replaces CC, with the Catalytic of Iron and Sodium elements more and more Flake shaped and fibrous like C-A-S-H 22gels generate due to the reaction between RM and MK (Fig. 13(5,6,7)) [43]. It is able to fill the pores between the cement particles to form a continuous gelling phase, which is easy to quickly obtain a certain strength in the early stages of hydration. On the whole, C-A-H and C-A-S-H gels can strengthen the structure, the flexural and compressive strengths increase, however, the setting time of LC^3 with RM is postponed.

Environmental benefit analysis

Herein, two optimal substitution ratios are examined: red mud replacing either 20% of kaolin or 15% of calcium carbonate. For every ton of cement produced, this approach can reduce the consumption of 200 kg of kaolin and the extraction of 150 kg of limestone, thereby decreasing reliance on natural resources. Kaolin requires low-temperature calcination treatment at 650 °C to 850 °C, resulting in CO_2 emissions of 105–167 kg per ton during its production process [44]. A 20% substitution with red mud can reduce CO_2 emissions by 21–33.4 kg for every ton of cement produced. Carbon emissions during the limestone treatment process primarily stem from the decomposition of calcium carbonate, with an emission factor of 440 kg/t [45]. A 15% substitution with red mud can reduce CO_2 emissions by 66 kilograms for every ton of cement produced. Additionally, each ton of cement can incorporate 150 to 200 kg of red mud.

Conclusion

This study focuses on various properties of mortars including fluidity, setting time, stability, mechanical properties, with LC^3 cement modified by RM. The effect of RM alkali diffusion on mortars is investigated by detection of EDS and pH value of the leaching solution, as well as the mineral composition and microstructure of mortars are detected by XRD and SEM. The following conclusions are gotten:

(1) The substitution of RM improves the fluidity of mortars, but with the RM increase, the fluidity decreases gradually. When RM replaces MK, the initial and final setting time of the mortars increase with more RM; when RM substitutes CC, the initial and final setting time decreases firstly and then increases with more RM. The LC^3 cement with RM is stable.

(2) The replacement of RM can significantly improve the compressive strength of mortars and influence the early development of flexural strength. The optimum MK replacement by RM is 20%, the resulting 28-d compressive strength is increased by 59.2%. The optimal CC substitution by RM is 15%, the resulting 28-day compressive strength is increased by 78.9%.

(3) The replacement of RM can increase the pH value of the leaching solution; addition of AC can decrease the pH value. According to EDS tests, RM addition causes calcium ions to migrate from the interior of mortars to the surface.

(4) According to the XRD and SEM detection, with the replacement of MK by RM, more C-A-H gels are generated and while RM replacement of CC, more C-A-S-H gels are prepared, which strengthens the mortars and postpones the setting time.

All in all, the replacement of MK and CC in LC^3 cement by RM can improve the detected properties of the LC^3 cement, especially, substitution of CC can satisfy the requirement the LC^3. The substitution of red mud can simultaneously achieve resource conservation, carbon emission reduction and solid waste disposal, providing a feasible path for the low-carbonization of the cement industry and waste recycling. In the future, further research should be conducted on the durability and the heat resistance property of red mud LC^3 cement [46], as well as the optimal dosage of ammonium carbonate and the control of its influence on performance. Although no marked performance decline was detected during the testing period, the outward migration of alkali metal ions indicates a potential long-term risk, wherein leaching could coarsen the pore network and adversely affect impermeability. Quantifying this effect via extended exposure or accelerated durability testing is necessary for future research.

CRediT authorship contribution statement

Yuwu Sui: Conceptualization, Methodology. Lingyu

Zhang, Xianglong Meng, Yiwei Fu: Visualization. Lingyu Zhang, Jialiang Wei, Zhixian Wang: Investigation, Data curation. Lingyu Zhang, Zhibo Zhang, Xiangman Deng: Writing - review & editing. Lingyu Zhang, Yuwu Sui, Shaoqi Zhang: Software.

Declaration of Competing Interest

The authors declare that they have no known competing financial interests or personal relationships that could have appeared to influence the work reported in this paper.

Acknowledgments

The Project is sponsored by the Shandong Province Key R&D Program (Public Welfare) 2019 (Grant Number: 2019GSF109108); The authors also thank to the help from Prof. Q.B. Tian and X. T. Yue.

References

1. F. Chen and T. Lou, China Cement. [09] (2020) 42-47. (in Chinese)
2. R.A. Berenguer, A.P. Capraro, M.H. de Medeiros, A.M. Carneiro, and R.A. De Oliveira, J. Environ. Chem. Eng. 8[2] (2020) 103655.
3. C.H. Peter, Lea's Chemistry of Cement and Concrete. (2003).
4. V. Sousa and J.A. Bogas, J. Cleaner Prod. 306 (2021) 127277.
5. K. Scrivener, F. Martirena, S. Bishnoi, and S. Maity, Cem. Concr. Res. 114 (2018) 49-56.
6. B. Kanagaraj, N. Anand, U.J. Alengaram, R.S. Raj, and S. Karthick, Resources, Conservation & Recycling Advances. 21 (2024) 200197.
7. H. Zhang, Master dissertation of Zhengzhou University. (2022) (in Chinese)
8. J. Chen, Master dissertation of Wuhan University of Technology. (2019) (in Chinese)
9. Z.Y. Huang, Y.S. Huang, W.Y. Liao, N.X. Han, Y.W. Zhou, F. Xing, T.B. Sui, B. Wang, H.Y. Ma, A.Z. Huang, and A.Y. Huang, Journal of Zhejiang University-Science A (Applied Physics & Engineering). 21[11] (2020) 892-907. (in Chinese)
10. S.L. Tang, Cement Engineering. [03] (2023) 1-6+18. (in Chinese)
11. W.Q. Cao, Master dissertation of Hubei University. (2023) (in Chinese)
12. Institute of Technical Information for Building Materials Industry, Jiangsu Building Materials. [04] (2019) 62. (in Chinese)
13. Y.Q. Shen, Master dissertation of Yangzhou University. (2022). (in Chinese)
14. T.T. Liang, Master dissertation of Shenzhen University. (2022). (in Chinese)
15. D. Yang, China Cement. [08] (2022) 69-71. (in Chinese)
16. Z.H. Xu, Master dissertation of Shenzhen University. (2022). (in Chinese)
17. L.J. Fu, China Cement. [09] (2020) 98-102. (in Chinese)
18. L.J. Fu, China Cement. [10] (2020) 91-93. (in Chinese)
19. N. Ijaz, W.M. Ye, Z. ur Rehman, Z. Ijaz, and M.F. Junaid, Sci. Total Environ. 907 (2024) 167794.
20. P. Yang, Y. Dhandapani, M. Santhanam, and N. Neithalath, Cem. Concr. Res. 130 (2020) 106010.
21. G. Mishra, A.C. Emmanuel, and S. Bishnoi, Materials and Structures. 52 (2019) 1-13.
22. C.H. Zhou, L.Z. Zhao, A.Q. Wang, T.H. Chen, and H.P. He, Appl. Clay Sci. 119 (2016) 3-7.
23. R.A. Schoonheydt, Appl. Clay Sci. 131 (2016) 107-112.
24. R. Kiew, A.R. Ummul-Nazrah, P.T. Ong, K. Imin, A.M. Aliaa-Athirah, and A.R. Rafidah, Journal of Tropical Forest Science. 31[1] (2019) 19-36.
25. S. Her, S. Im, J. Liu, H. Suh, G. Kim, S. Sim, K. Wi, D. Park, and S. Bae, Constr. Build. Mater. 425 (2024) 135918.
26. H. Alghamdi, H. Shoukry, A.A. Abadel, and M. Khawaji, J. Mater. Res. Technol. 23 (2023) 2065-2074.
27. Y. Hu, L. Xiong, Y. Yan, and G. Geng, Case Studies in Construction Materials. 20 (2024) e03283.
28. J. Hu, R. Niu, W. Zhang, G. Xie, J. Liu, and F. Xing, Constr. Build. Mater. 438 (2024) 137040.
29. P. Du, P. Wang, X. Zhang, G. Wen, and Y. Wang, Particuology. 93 (2024) 328-348.
30. N. Zhang, X. Guo, Y. Li, J. Zhang, and T. Yu, J. Ceram. Process. Res. 25[3] (2024) 355-364.
31. W. Cui, Q. Cui, X. Dong, J. Liu, K. Song, M. Xie, and X. Yao, Constr. Build. Mater. 442 (2024) 137605.
32. J. Wang, K. Xu, Z. Li, Y. Yang, Q. Li, Y. Bao, H. Yang, L. Ding, R. Zhang, Y. Wang, and L. Yao, J. Ceram. Process. Res. 23[1] (2022) 79-85.
33. N.T. Tran, D.V.Q. Nguyen, V.M.H. Ho, X.T. Dang, and N.Q. Tran, J. Ceram. Process. Res. 18[5] (2017) 366-372.
34. V. Shirodkar, R. Patel, M. Verma, and V. Mahate, Mater. Today: Proc. (2023).
35. L. Tang, Z. He, R. Yang, S. Pei, M. Zou, and M. Qin, Sustainable Chem. Pharm. 41 (2024) 101717.
36. C. Hu, W. Xiang, P. Chen, Y. Yang, L. Zhou, J. Jiang, S. Li, M. Yang, and Q. Li, J. Renewable Mater. 11[11] (2023) 3945.
37. Y. Xiao, Y. Jiang, B. Chen, and L. Wang, Constr. Build. Mater. 409 (2023) 134023.
38. Chinese National Bureau of Quality Supervision, GB/T 2419 (2005) (in Chinese)
39. The State Administration for Market Regulation of China, JJF 1867 (2020) (in Chinese)
40. Chinese National Bureau of Quality Supervision, GB/T 17671 (2021) (in Chinese)
41. Chinese National Bureau of Quality Supervision, GB/T 1346 (2011) (in Chinese)
42. M. Antoni, J. Rossen, F. Martirena, and K. Scrivener, Cem. Concr. Res. 42[12] (2012) 1579-1589.
43. Y. Yu, Master dissertation of Nanchang University. (2024)
44. T. Tasiopoulou, D. Katsourinis, D. Giannopoulos, and M. Founti, Eng. 4[1] (2023) 761-779.
45. IPCC, 2006 IPCC Guidelines for National Greenhouse Gas Inventories, 3[Industrial Processes and Product Use] (2006).
46. G. Meng, Y. Sui, S. Liu, Q. Tian, X. Cui, and Y. Wu, J. Ceram. Process. Res. 23[6] (2022) 831-838.